Electronic Supplementary Information

As-cast ternary polymer solar cells based on a nonfullerene acceptor and its fluorinated counterpart showing improved efficiency and good thickness tolerance

Feilong Pan, Lianjie Zhang, Haiying Jiang, Dong Yuan, Yaowen Nian, Yong Cao and Junwu Chen*

Institute of Polymer Optoelectronic Materials & Devices, State Key Laboratory of Luminescent Materials & Devices, South China University of Technology, Guangzhou 510640, P. R. China.

Materials

PBDB-T-SF, IDIC and PDIN were purchased from Solarmer Materials (Bejing) Inc. ID4F was purchased from Derthon. The processing solvents used in the device fabrication processes were purchased from Alfa Aesar and used as received.

Device fabrication

All PSCs with conventional structure were fabricated with the structure of ITO/PEDOT:PSS/active layer/PDIN/Al. The patterned ITO-coated glass substrates with a sheet resistance of 15-20 ohm square^{-1} were cleaned by sequential sonication using detergent, acetone, deionized water, and ethanol, and dried in oven at 70 °C before used. After oxygen plasma cleaning for 4 min, a 40 nm thick PEDOT:PSS (Clevios P Al4083) anode buffer layer was spun onto the substrates and annealed at 150 °C on a hot plate for 15 min. then the substrates were transferred into a nitrogen-filled glove box. The PBDB-T-SF:IDIC and PBDB-T-SF:ID4F with 1:1 weight ratio were dissolved in chlorobenzene to prepare 10 mg/mL binary blend solutions, respectively. After heated and stirred at 75 °C about 3 h, binary blend solutions were mixed by different volume ratios to obtain ternary blend solutions of PBDB-T-SF$_{100}$:IDIC$_{100-x}$:ID4F$_x$ (x=0, 10, 30, 40,

50, 70, 90, 100 wt%, x represents ID4F content in acceptors). Subsequently, the prepared blend solutions were spin-coated on PEDOT:PSS modified ITO substrates at 1500 rpm for 50 s gave the film with thickness of about 100 nm. The methanol solution (0.3% acetic acid) of PDIN at a concentration of 1.5 mg/mL was spin-coated onto active layers at 3000 rpm for 30 s to prepare cathode interlayer. Finally, 100 nm aluminum (Al) was thermally deposited on top of the interface through a shadow mask in a vacuum chamber at a pressure of 2×10^{-4} Pa. The active layer area of the device was defined to be 0.058 cm^2.

Instruments and Characterization

UV−vis absorption spectra were recorded on an HP 8453 spectrophotometer. Cyclic voltammetry was carried out on a CHI660A electrochemical work station with platinum electrodes at a scan rate of 50 mV/s against an Ag/Ag^+ reference electrode with a nitrogen-saturated solution of 0.1 M tetrabutylammonium hexafluorophosphate (Bu4NPF6) in acetonitrile. Potentials were referenced to the ferrocenium/ferrocene couple by using ferrocene as an internal standard. The deposition of a copolymer on the electrode was done by the evaporation of a dilute chloroform solution. Differential scanning calorimetry (DSC) analysis was performed on a NETZSCH (DSC200F3) apparatus at a heating rate of 5 °C /min under a nitrogen atmosphere. The thickness values of the PEDOT:PSS and active layer were verified by a surface profilometer (Tencor, Alpha-500). The thickness of the evaporated cathodes was monitored by a quartz crystal thickness/ratio monitor (Model: STM-100/MF, Sycon). The photovoltaic performance was measured under an AM 1.5G (air mass 1.5 global) spectrum from a solar simulator (Japan, SAN-EI, XES-40S1) (100 Mw/cm^2). The current density-voltage (*J-V*) characteristics were recorded with a Keithley 2400 source meter. The light intensity of the light source was calibrated before the testing by using a standard silicon solar cell with a KG5 filter, as calibrated by a National Renewable Energy Laboratory (NREL) certified silicon photodiode, giving a value of 100 mW/cm^2 in the test. The external quantum efficiency (EQE) spectra were performed on a commercial EQE measurement system (Taiwan, Enlitech, QE-R3011). The light intensity at each wavelength was calibrated by a standard single-crystal Si photovoltaic

cell. Tapping-mode AFM images were obtained by using a Bruker Multimode 8 Microscope. Transmission electron microscopy (TEM) images were obtained by using a JEM 2100F Microscope. For TEM measurements, the preparation of samples was carried out through the wetting transfer method. The active layers were spin-coated onto the PEDOT:PSS modified ITO substrates and then the substrates were immersed into deionized water. After the active layers up-floated, a copper grid was used to hold up the up-floated active layers by a sharp tweezers. The samples were transferred into vacuum to evaporate the water before testing.

Grazing incidence X-ray diffraction (GIXD) experiments were carried out on a Xenocs Xeuss 2.0 system with an Excillum MetalJet-D2 X-ray source operated at 70.0 kV, 2.8570 mA, and a wavelength of 1.341 Å. The grazing-incidence angle was set at 0.20°. Scattering pattern was collected with a Dectris Pilatus3R 1M area detector.

Hole-only and electron-only devices were fabricated to measure the hole and electron mobilities of active layers by using the space charge limited current (SCLC) method with hole-only devices of ITO/PEDOT:PSS/Active layer/MoO_3/Al and electron-only devices of ITO/Al/Active layer/Ca/Al. The mobilities (μ_h or μ_e) were determined by fitting the dark current to the model of a single carrier SCLC, described by the equation:

$$J = \frac{9}{8}\varepsilon_0\varepsilon_r\mu\frac{V^2}{d^3}$$

Where J is the current, ε_0 is the permittivity of free space, ε_r is the material relative permittivity, d is the thickness of the active layer and V is the effective voltage. The effective voltage can be obtained by subtracting the built-in voltage (V_{bi}) from the applied voltage (V_{appl}), $V=V_{appl}-V_{bi}$. The mobility can be calculated from the slope of the $J^{1/2}$-V curves.

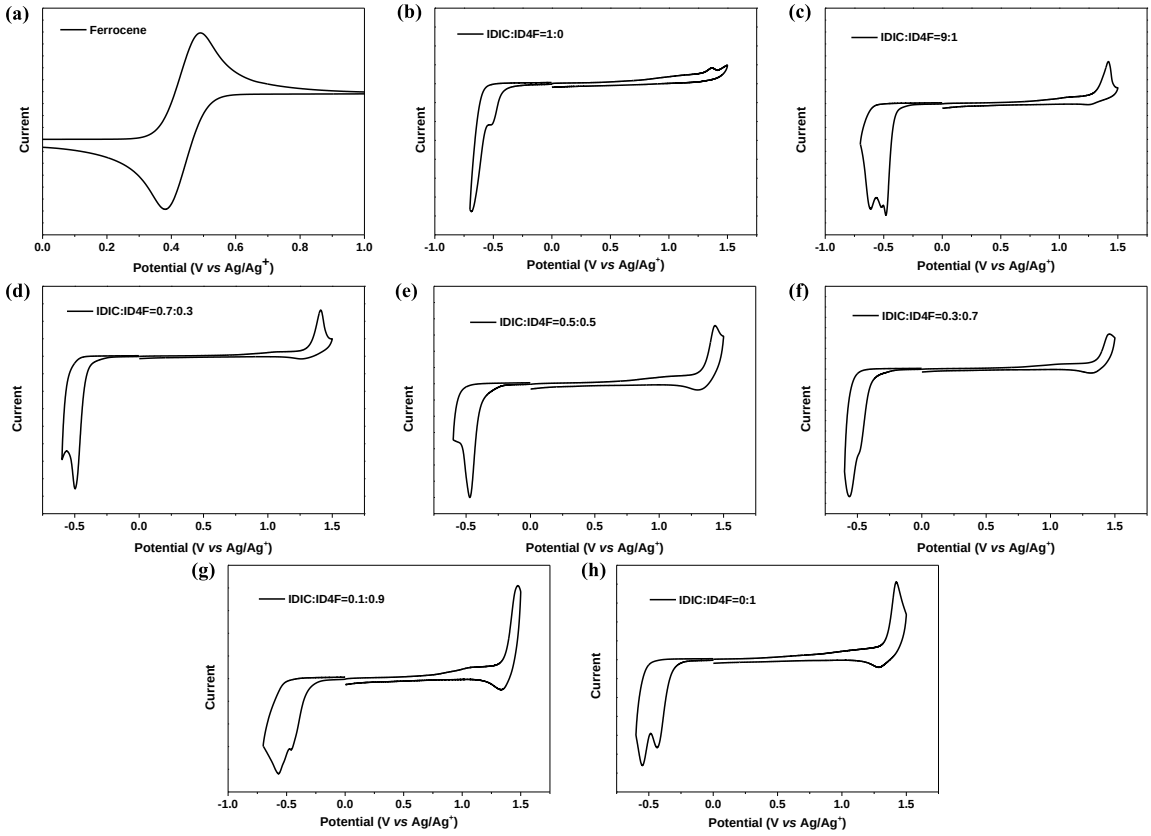

Fig. S1. Cyclic voltammograms of IDIC:ID4F blend films with different ID4F content on a glassy carbon electrode measured in a 0.1 mol/L Bu_4NPF_6 acetonitrile solution at a scan rate of 50 mV/s.

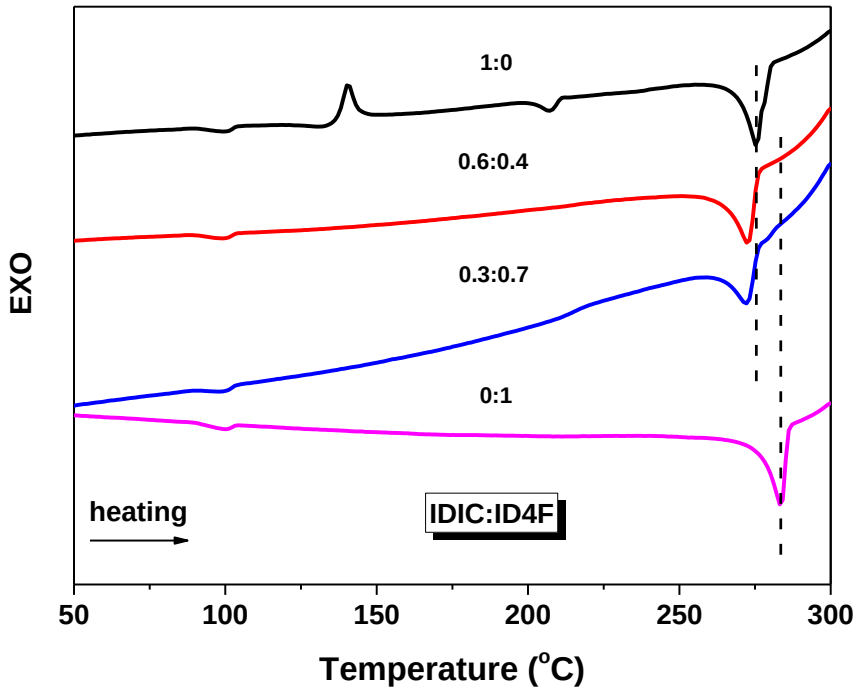

Fig. S2. DSC curves of the IDIC:ID4F blend films with different blend ratios at a scan rate of 5 °C/min under nitrogen atmosphere.

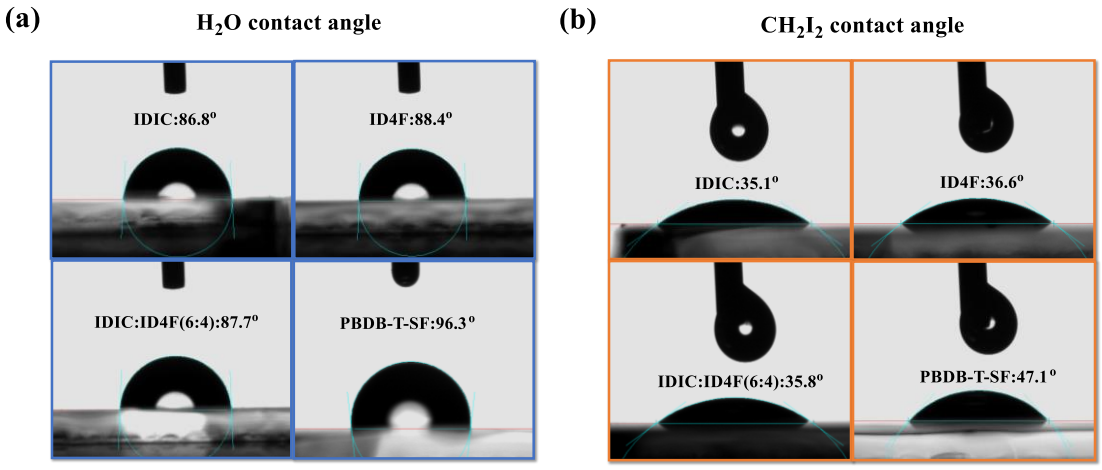

Fig. S3. The images of contact angles of IDIC, ID4F, IDID:ID4F (6:4), and PBDB-T-SF neat films using different liquid: (a) H_2O and (b) CH_2I_2.

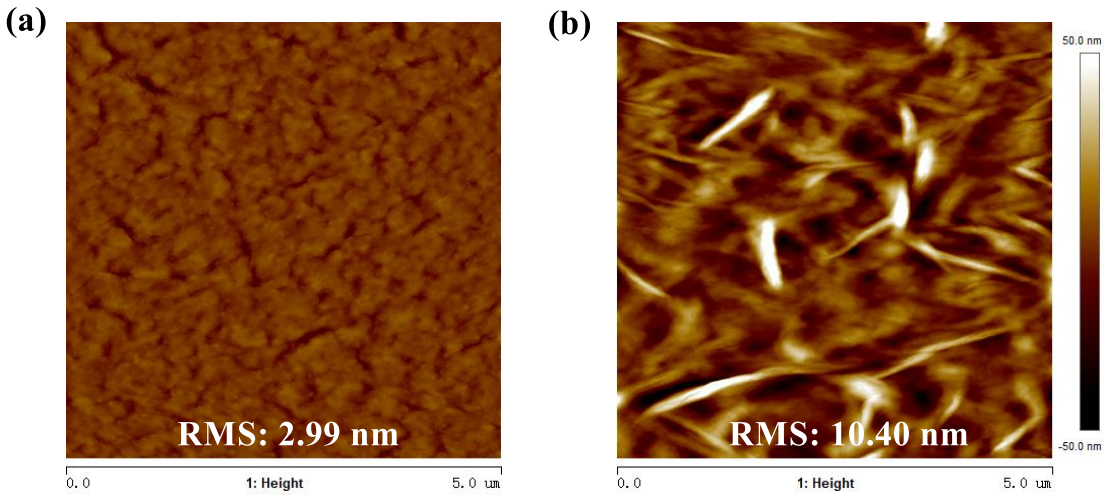

Fig. S4. AFM images of neat acceptor films for (a) IDIC and (b) ID4F.

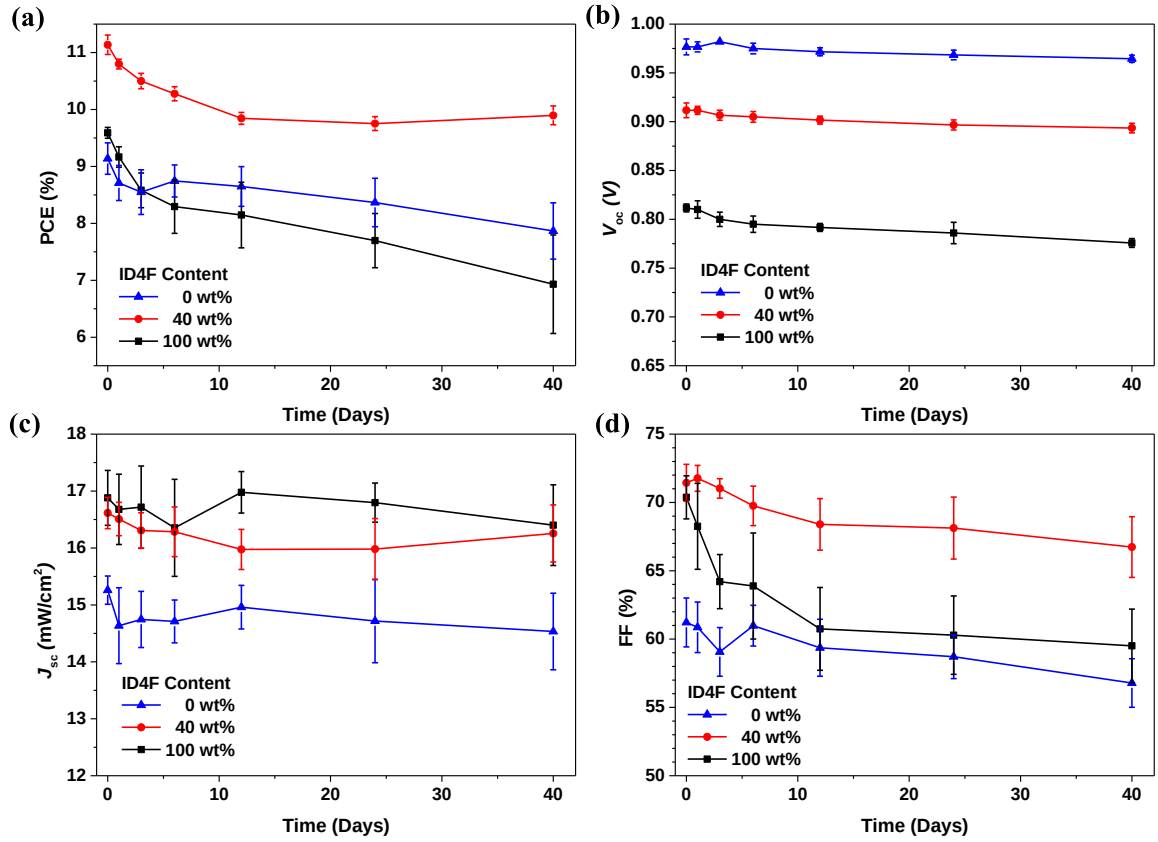

Fig. S5. The dependence of (a) PCE, (b) V_{oc}, (c) J_{sc}, and (d) FF on storage time for the binary and ternary PSCs in nitrogen-filled glovebox.

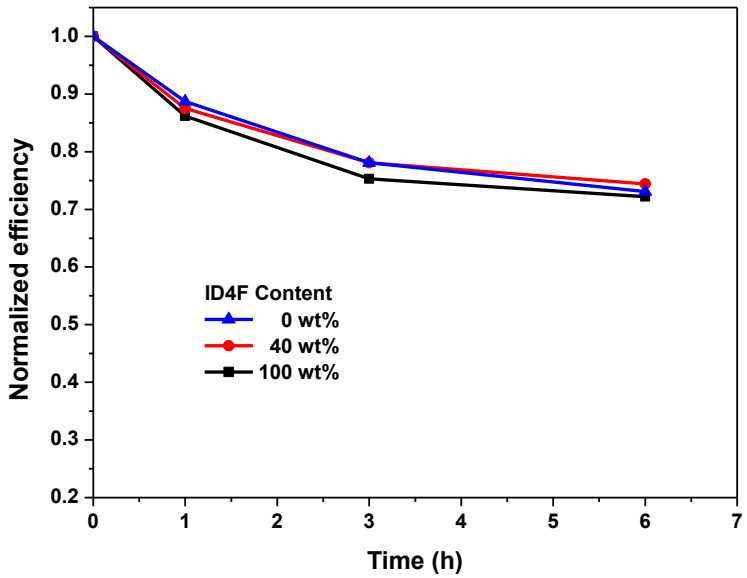

Fig. S6. The photostability of the binary and ternary PSCs with encapsulation under an AM 1.5G (air mass 1.5 global) spectrum from a solar simulator in air.

Table S1. Summary of ternary PSCs with thick films reported in literatures.

Ternary system	Binary blend	The third component	Extra treatment	PCE(%)/ thickness	Reference
D1:D2:A	PCE10:$PC_{71}BM$	BTR	SA	10.16 / (100nm) 10.30 / (250nm)	1
	PffBT4T-2OD:$PC_{71}BM$	BTR	SA+TA	/ (100nm) 10.59 / (280nm)	2
	PNTT:$PC_{71}BM$	BTR	SA+TA	/ (100nm) 11.44 / (280nm)	2
	PTB7-Th:$PC_{71}BM$	p-DTS$(FBTTH_2)_2$	SA	10.17 / (100nm) 10.78 / (200nm)	3
	PTB7-Th:$PC_{71}BM$	FTR	SA	9.4 / (160nm) 8.2 / (200nm)	4
	PTB7-Th:$PC_{71}BM$	PBTZT-STAT-BDTT-8	SA	10.2 / (100nm) 11.03 / (260nm)	5
	PTB7:$PC_{71}BM$	p-DTS$(FBTTH_2)_2$	/	8.1 / (120nm) 7.6 / (200nm)	6
	PEG-2%:N2200	PTB7-Th	SA+TA	9.27 / (130nm) 8.05 / (240nm)	7
	PBTA-Si:N2200	PTzBI-Si	TA	9.56 / (150nm) 9.17 / (350nm)	8
	PTzBI:N2200	PBTA-BO	SA+TA	10.12 / (130nm) 9.01 / (304nm)	9
	PBTA-BO:N2200	PNTB	SA+TA	9.87 / (130nm) 6.66 / (270nm)	10
D:Fullerene:Nonfullerene	PBODT:$PC_{71}BM$	ITIC	/	7.22 / (100nm) 8.42 / (300nm)	11
	PDOT:$PC_{71}BM$	ITIC	SA	9.55 / (97nm) 10.87 / (275nm)	12
	BTR:$PC_{71}BM$	NITI	SVA	10.58 / (150nm) 13.20 / (300nm)	13
	DR3:ICC6	$PC_{71}BM$	SVA	/ (100nm) 10.8 / (200nm)	14
D:Nonfullerene 1:Nonfullerene 2	PBDB-T-SF:IDIC	ID4F	/	11.52 / (100nm) 10.05 / (250nm)	**This work**

SA is solvent additive; TA is thermal annealing; SVA is solvent vapor annealing.

Table S2. The E_{red}, E_{ox}, HOMO and LUMO energy levels of IDIC:ID4F blend films with different ID4F content extracted from the corresponding CV curves

ID4F Content (wt%)	E_{red} (V)	E_{ox} (V)	LUMO (eV)	HOMO (eV)
0	−0.4334	1.2948	3.9311	5.6593
10	−0.4162	1.2981	3.9483	5.6626
30	−0.4099	1.3044	3.9546	5.6689
50	−0.3950	1.3239	3.9695	5.6884
70	−0.3674	1.3413	3.9971	5.7058
90	−0.3295	1.3511	4.0350	5.7156
100	−0.3188	1.3531	4.0457	5.7176

Table S3. The contact angles of different liquids and surface energies of IDIC, ID4F, IDIC:ID4F (0.6:0.4), and PBDB-T-SF films.[a]

Materials	θ_{water} (deg)	θ_{DIM} (deg)	γ^d (mJ/m^2)	γ^p (mJ/m^2)	Surface energy[b] (mJ/m^2)
IDIC	86.8	35.1	38.44	5.93	44.37
ID4F	88.4	36.6	37.95	5.36	43.31
IDIC:ID4F	87.7	35.8	38.20	5.60	43.80
PBDB-T-SF	96.3	47.1	34.14	3.07	37.21

[a] DIM is diiodomethane (CH_2I_2), γ^d is the dispersion component of surface energy, and γ^p is the polar component of surface energy. [b] The surface energy is calculated according to the Wu model.[15]

Table S4. Relevant parameters obtained from J_{ph}-V_{eff} curves

ID4F content (wt%)	J_{sat} (mA/cm^2)	J_{ph} (mA/cm^2)	G_{max} (m^{-3}s^{-1})	*P(E,T)* (%)	*L* (nm)
0	16.18	15.13	0.91×10^{28}	93.51	111
40	17.47	16.43	1.01×10^{28}	94.02	108
100	17.83	17.09	1.04×10^{28}	95.85	107

Table S5. The photovoltaic performance of the devices based on PBDB-T-SF:ID4F (40 wt%):IDIC with different thickness[a]

Thickness (nm)	V_{oc} (V)	J_{sc} (mA/cm^2)	FF (%)	PCE (%)
85	0.917	16.27	73.28	10.93
	(0.915±0.006)	(16.26±0.32)	(72.12±1.09)	(10.73 ± 0.18)
100	0.917	16.89	74.35	11.52
	(0.918±0.005)	(16.64±0.34)	(73.23±1.04)	(11.18 ± 0.16)
150	0.900	17.48	69.92	11.00
	(0.910±0.006)	(17.07±0.39)	(69.68±1.80)	(10.82±0.23)
200	0.908	17.15	67.62	10.53
	(0.902±0.005)	(17.04±0.10)	(65.05±2.69)	(10.00±0.50)
250	0.900	17.06	65.43	10.05
	(0.905±0.005)	(16.99±0.17)	(63.16±2.66)	(9.71±0.43)

[a] The average values are based on 15 devices

Reference

1. G. Zhang, K. Zhang, Q. Yin, X.-F. Jiang, Z. Wang, J. Xin, W. Ma, H. Yan, F. Huang and Y. Cao, *J. Am. Chem. Soc.*, 2017, **139**, 2387-2395.
2. M. Xiao, K. Zhang, Y. Jin, Q. Yin, W. Zhong, F. Huang and Y. Cao, *Nano Energy*, 2018, **48**, 53-62.
3. J. Zhang, Y. Zhao, J. Fang, L. Yuan, B. Xia, G. Wang, Z. Wang, Y. Zhang, W. Ma and W. Yan, *Small*, 2017, **13**, 1700388.
4. X. Fu, H. Xu, D. Zhou, X. Cheng, L. Huang, L. Chen and Y. Chen, *J. Mater. Sci.*, 2018, **53**, 8398-8408.
5. N. Gasparini, L. Lucera, M. Salvador, M. Prosa, G. D. Spyropoulos, P. Kubis, H.-J. Egelhaaf, C. J. Brabec and T. Ameri, *Energy Environ. Sci.*, 2017, **10**, 885-892.
6. H. Yin, S. H. Cheung, J. H. Ngai, C. H. Y. Ho, K. L. Chiu, X. Hao, H. W. Li, Y. Cheng, S. W. Tsang and S. K. So, *Adv. Electron. Mater.*, 2017, **3**, 1700007.
7. Z. Li, B. Fan, B. He, L. Ying, W. Zhong, F. Liu, F. Huang and Y. Cao, *Sci. China Chem.*, 2018, **61**, 1-10.
8. B. Fan, P. Zhu, J. Xin, N. Li, L. Ying, W. Zhong, Z. Li, W. Ma, F. Huang and Y. Cao, *Adv. Energy Mater.*, 2018, **8**, 1703085.
9. Z. Li, L. Ying, R. Xie, P. Zhu, N. Li, W. Zhong, F. Huang and Y. Cao, *Nano Energy*, 2018, **51**, 434-441.
10. Z. Li, R. Xie, W. Zhong, B. Fan, J. Ali, L. Ying, F. Liu, N. Li, F. Huang and Y. Cao, *Solar RRL*, 2018, **2**, 1800196.
11. Z. Wang, H. Jiang, L. Zhang, X. Liu, J. Sun, Y. Cao and J. Chen, *Org. Electron.*, 2018, **61**, 359-365.
12. T. Zhang, X. Zhao, D. Yang, Y. Tian and X. Yang, *Adv. Energy Mater.*, 2018, **8**, 1701691.
13. Z. Zhou, S. Xu, J. Song, Y. Jin, Q. Yue, Y. Qian, F. Liu, F. Zhang and X. Zhu, *Nat. Energy*, 2018, **3**, 952.
14. R. Z. Liang, Y. Zhang, V. Savikhin, M. Babics, Z. Kan, M. Wohlfahrt, N. Wehbe, S. Liu, T. Duan and M. F. Toney, *Adv. Energy Mater.*, 2018, **9**, 1802836.
15. K.-H. Kim, H. Kang, H. J. Kim, P. S. Kim, S. C. Yoon and B. J. Kim, *Chem. Mater.*, 2012, **24**, 2373.